

## ARTICLE



# Bone mesenchymal stem cell-derived extracellular vesicles containing NORAD promote osteosarcoma by miR-30c-5p

Hongtao He<sup>1</sup>, Muliang Ding<sup>2</sup>, Tao Li<sup>3</sup>, Wenzhi Zhao<sup>1</sup>, Lu Zhang<sup>1</sup>, Peng Yin<sup>1</sup> and Wei Zhang<sup>4✉</sup>

© The Author(s), under exclusive licence to United States and Canadian Academy of Pathology 2022, corrected publication 2022

Osteosarcoma is a bone tumor that often affects children, adolescents and young people. Non-coding RNA activated by DNA damage (NORAD) can promote the proliferation of cancer cells in multiple tumors. Thus, the current study set out to explore the role of NORAD derived from extracellular vesicles (EVs) of bone mesenchymal stem cells (BMSCs) in osteosarcoma. First, NORAD was highly expressed in osteosarcoma cells and tissues, which might be associated with the progression and metastasis of osteosarcoma. We isolated EVs from the characterized BMSCs, and found that NORAD was transferred from BMSCs to osteosarcoma cells *via* EVs in the co-culture system. Consequently, NORAD delivered by BMSC-derived EVs promoted the proliferation and invasion of osteosarcoma cells. Subsequently, bioinformatics analyses suggested potential binding relationship between NORAD and microRNA-30c-5p (miR-30c-5p) as well as between miR-30c-5p and Krueppel-like factor 10 (KLF10), and the results of which were further verified by dual luciferase reporter gene assay, RNA immunoprecipitation, and RNA pull-down assay. Mechanistically, NORAD acted as a sponge of miR-30c-5p and up-regulated the expression of KLF10 where miR-30c-5p mimic declined the effect induced by NORAD on cancer cells. The osteosarcoma cells were injected into mice to develop tumor growth and metastasis models. In these two models, injection of BMSC-EVs elevated NORAD expression and KLF10 but reduced miR-30c-5p expression, whereby suppressing tumor growth and lung metastasis. To conclude, BMSC-EVs deliver NORAD to osteosarcoma cells to regulate the miR-30c-5p/KLF10 axis, thereby accelerating the progression and metastasis of osteosarcoma.

*Laboratory Investigation* (2022) 102:826–837; <https://doi.org/10.1038/s41374-021-00691-6>

## INTRODUCTION

Osteosarcoma originates from the mesenchyme, and is the most commonly diagnosed primary malignant bone tumor across the world [1]. Children and adults are most frequently affected by osteosarcoma [2], and the malignancy is associated with multiple gene mutation diseases, such as Rothmund-Thomson syndrome, Li-Fraumeni syndrome, and Bloom syndrome [3]. In addition to genetic mutations, the increased risk of osteosarcoma is also related to gender [4], age [5], height [6], and metastasis [7]. Moreover, the outcome of patients with distant metastases remains poor, with 5-year survival rate being only 13% [8]. Nevertheless, current chemotherapeutic regimens have significantly augmented patient 5-year tumor-free survival rate to 70%; however, the side effects and drug resistance of chemotherapy and the spread of tumors still persist as clinical obstacles [9]. Therefore, it would be prudent to further clarify the potential molecular mechanism of osteosarcoma and identify new biomarkers in order to develop a novel targeted therapeutic regimen for osteosarcoma [10].

In recent years, an increasing number of studies have shown that the tumor microenvironment (TME) plays an important role in tumor progression [11, 12]. Bone mesenchymal stem cells (BMSCs) are one of the major components in the TME of osteosarcoma, and have also been shown to mediate cell proliferation and

metastasis in various malignancies [13]. Furthermore, various cell types including BMSCs are known to secrete extracellular vesicles (EVs). These EVs communicate between the cells by packaging and transferring active molecules such as proteins, messenger RNA (mRNA) and non-coding RNAs from one cell to another [14]. More importantly, recent studies have shown that BMSC-derived EVs play critical roles in the proliferation and migration of tumor cells [15]. In addition, the study performed by Qi et al. has demonstrated that BMSC-derived EVs possess the ability to promote the growth of osteosarcoma cells [16]. Also, BMSC-derived EVs have been reported to transfer long non-coding RNA (lncRNA) plasmacytoma variant translocation 1 (PVT1) to facilitate tumor growth and metastasis in osteosarcoma [17].

Of many of the lncRNAs correlated with human cancers, noncoding RNA activated by DNA damage (NORAD) is known to be dysregulated in various types of human carcinomas, including osteosarcoma [18]. It has been suggested that lncRNAs may act as competing endogenous RNAs (ceRNAs) to exert cancer-promoting effects [19]. Meanwhile, microRNA-30c-5p (miR-30c-5p) was recently highlighted to suppress apoptosis and inflammatory response in endothelial cells [20]. In addition, down-regulated expression levels of miR-30c-5p were previously documented in osteosarcoma tissues [21]. More importantly, in human osteosarcoma, NORAD can regulate tumor proliferation and migration by

<sup>1</sup>Department of Traumatic Orthopedics, The Second Hospital of Dalian Medical University, Dalian 116023, China. <sup>2</sup>Department of Orthopedics, The Second Xiangya Hospital, Central South University, Changsha 410011, China. <sup>3</sup>Department of Orthopedics, Renji Hospital Affiliated to Shanghai Jiaotong University School of Medicine, Shanghai 200092, China. <sup>4</sup>Department of Spine Surgery, The Second Hospital of Dalian Medical University, Dalian 116023, China. ✉email: zhangwei1983@dmu.edu.cn

Received: 29 October 2020 Revised: 11 October 2021 Accepted: 18 October 2021

Published online: 24 March 2022

competitively binding to miR-199a-3p [22]. However, it is still unclear whether NORAD participates in the functional regulation of cancer development in osteosarcoma through miR-30c-5p *via* EVs. Consequently, the current study set out to explore the role of BMSC-EVs delivered NORAD and the miR-30c-5p/Kruppel Like Factor 10 (KLF10) axis in regard to osteosarcoma cells.

## MATERIALS AND METHODS

### Ethical statement

Protocols for the current study were approved by the Second Hospital of Dalian Medical University's Ethics Committee, and conformed to the guidelines of the Declaration of Helsinki. Signed informed consents were obtained from all participants. All animal experiments were in accordance with ethical standards and approved by the Animal Ethics Committee of the Second Hospital of Dalian Medical University, and extensive efforts were made to minimize the suffering of the included animals.

### Clinical specimens

First, a total of 30 paired osteosarcoma tissues and adjacent tissue specimens were obtained from patients diagnosed with osteosarcoma by histopathological evaluation at the Second Hospital of Dalian Medical University. None of the included 11 patients received treatment prior to specimen collection. Clinical characteristics of the enrolled patients are shown in Table S1. Human BMSCs were isolated from three donated bone marrow by reference to previous methods [23], and the diagnosis was based on magnetic resonance imaging without damaged femoral head and diseases such as trauma, blood system diseases, tuberculosis and tumor infiltration.

### Cell culture

Osteosarcoma cell lines 143B (CRL-8303), HOS (CRL-1543), Saos-2 (HTB-85) and MG-63 (CRL-1427) were procured from the American Type Culture Center (Manassas, VA, USA). In addition, the human osteoblast hFOB 1.19 was purchased from the Cell Bank of the Chinese Academy of Sciences (Shanghai, China). Subsequently, the cells were identified by means of short tandem repeat DNA analysis and regularly checked for mycoplasma contamination. Next, MG-63 and hFOB 1.19 cell lines were incubated in Dulbecco's modified Eagle medium (DMEM)/F12 (Gibco, NY, USA), 143B and Saos-2 cell lines in DMEM (Gibco), and the HOS cell lines in DMEM and MEM (Gibco). The medium used in this study was supplemented with 10% (v/v) fetal bovine serum (FBS, Sigma, St. Louis, USA), 100 IU/mL penicillin (Sigma) and 100 mg/mL streptomycin (Sigma). The osteosarcoma cell line was cultured in a humidified incubator at 37 °C with 5% CO<sub>2</sub>.

### Plasmid construction and cell transfection

Lentiviral particles expressing NORAD (pLenti-NORAD, Lv-NORAD), negative control (Lv-NC), short hairpin RNA (sh)NORAD (pLenti-sh-NORAD), or negative control (shNC) (final concentration: 100 nM) were packaged into HEK-293T cells using lentiviral packaging kits (Invitrogen, Carlsbad, CA, USA). After 48 h, the virus supernatant was collected and concentrated with Genechem (Shanghai, China). After the cell confluence of 143B, MG-63 and BMSCs reached about 50%, the cells were then infected with lentivirus ( $1 \times 10^8$  TU/mL) and 48 h after infection, the cells were screened with 10 µg/mL puromycin (Sigma) for at least 1 week to select the stably-transfected cell lines. shRNA sequence: shControl: CAACAAGATGAAGAGC ACCAA; sh-NORAD #1: GCCGACGTATGATAAATAGA; sh-NORAD #2: GGGG TGACAACTTATGATAAAA. The sequence with the highest interference efficiency (sh-NORAD #1) was selected for subsequent experimentation.

For transient transfection, shKLF10, miR-30c-5p mimic and miR-30c-5p inhibitor and corresponding controls were purchased from Genechem. Next, the osteosarcoma cells were inoculated in a 6-well plate at a density of  $4 \times 10^5$  cells/mL, and when the cell confluence reached about 80%, the cells were transfected with shKLF10, miR-30c-5p mimic and miR-30c-5p inhibitor and corresponding controls according to lipofectamine 2000 kit instructions (11668-019, Invitrogen). Briefly, 25 pmol mimic/inhibitor was diluted with 250 µL serum-free Opti-MEM (51985042, Gibco). Then, 10 µL Lipofectamine 2000 was diluted with 250 µL serum-free Opti-MEM. The aforementioned diluted mimic/inhibitor was mixed and allowed to stand for 20 min and added into the culture wells. Following transfection, the cells were cultured at 37 °C with 5% CO<sub>2</sub> for 48 h for subsequent experimentation.

### Isolation of BMSCs and identification of multi-differentiation potential

The isolated BMSCs were cultured in DMEM-F12 basal medium (HyClone Company, Logan, UT, USA) containing 10% FBS (10099141, Gibco), 0.2% penicillin and streptomycin (HyClone). The BMSCs were passaged every 3 days until BMSCs at passage 3–7 were obtained. Then, the obtained BMSCs were cultured in OriCell™ BMSC osteogenic, adipogenic or chondrogenic differentiation medium (Cyagen, Guangzhou, China), and were, respectively, stained with 0.5% oil red O solution, 5% silver nitrate solution, or 1% Alcian blue solution staining to evaluate intracellular lipid droplets, calcium deposition, or proteoglycan accumulation.

### Separation and purification of EVs

FBS was ultracentrifuged and centrifuged at 100,000 × g for 18 h to remove EVs. When BMSCs reached about 80% confluence, the medium was replaced with 10% FBS medium with EVs removed, and the BMSCs were cultured in an incubator at 37 °C with CO<sub>2</sub> for 48 h. The collected culture supernatant was then centrifuged at 500 × g for 15 min, decellularized at 4 °C at 2000 × g for 15 min to remove debris or apoptotic bodies at 4 °C, and at 10,000 × g for 20 min at 4 °C to remove large vesicles. Next, the supernatant was filtered with a 0.22 µm filter, centrifuged at 110,000 × g for 70 min at 4 °C, resuspended in PBS and ultracentrifuged in the same conditions, then resuspended in 100 µL of sterile PBS for downstream experiments. All ultracentrifuges were performed using a Beckman ultracentrifuge (Optima L-90K, USA) equipped with a SW-32Ti rotor and centrifuges using Beckman Allegra X-15R benchtop centrifuges.

### Identification of EVs

First, 20 µg EVs were dissolved in 1 mL PBS, vortexed for 1 min to maintain uniform distribution of EVs, followed by the measurement of size distribution with NanoSight Nanoparticle Tracking Analyzer (NTA, Malvern Instruments Co., Ltd., UK).

For observation under transmission electron microscope (TEM), 20 µL of fresh samples of ultra-separated EVs were loaded onto a carbon-coated copper electron microscope grid for 2 min and stained for 5 min with phosphotungstic acid solution (12501-23-4, Sigma). Next, the grid was rinsed three times with PBS to remove the excess phosphotungstic acid solution, and then kept semi-dry with a filter paper. A TEM (H7650, Hitachi, Japan) was used to observe the image at 80 KV.

For the identification of markers of EVs, the EV suspension was concentrated and the protein content was determined using a bicinchoninic acid (BCA) kit (23227, Thermo Fisher Scientific, MA, USA). Next, the proteins were subjected to sodium dodecyl sulfate-polyacrylamide gel electrophoresis, transferred onto a membrane, and the expression patterns of EV-specifically labeled TSG101 (ab30871, Abcam, Cambridge, UK), CD81 (ab79559, Abcam), Alix (ab76608, abcam), glucose-regulated protein 94 (GRP94) (ab3674, Abcam), and apolipoprotein B (APOB) (ab20737, Abcam).

### Verification of loading of NORAD into EVs

RNase A treatment was performed to determine whether lncRNA was surface bonded to the EVs or packaged into EVs. In short, the EVs were resuspended in PBS and incubated with 20 µg/µL RNase A (Purelink RNase A, Thermo Fisher Scientific) at 37 °C for 20 min. Following treatment with detergent (TritonX-100) to destroy the vesicle membrane, the EVs were then incubated with Radio Immunoprecipitation Assay (RIPA) buffer for 20 min, with RNase A, and then with lysis buffer. Finally, RNA content was isolated and the relative expression patterns of NORAD were measured.

### Cell uptake of EVs

First, the purified BMSC-EVs were labeled with PKH67 Green Fluorescence kits (Sigma). Next, the EVs were resuspended in  $4 \times 10^{-6}$  M dye solution containing 1 mL Diluent C solution and 4 µL of PKH67 ethanol dye solution for 5 min, and then incubated with 2 mL of 1% FBS without EVs for 1 min to stop staining. The labeled EVs were then ultracentrifuged at 100,000 × g for 2 h [24]. The osteosarcoma cells were subsequently incubated with PKH67-EVs for 12 h at 37 °C, fixed with 4% paraformaldehyde, and stained with 4',6-diamino-2-phenylindole (D9542, Sigma). Finally, the uptake of EVs by osteosarcoma cells was observed under a fluorescence microscope (ECLIPSE E800, Nikon, Japan).

In order to explore the transfer of NORAD, fluorescein isothiocyanate (FITC)-NORAD was electrically-transfected to EVs, which was isolated from 300 µL of MSC culture conditioned medium. Briefly, 200 ng EVs were added with 400 µL electroporation buffer (21% Optiprep, 25 mM KCl,

100 mM potassium phosphate, pH 7.2) and 30 µg FITC-NORAD, transferred to 4 mm electroporation test tube (Eppendorf, Hauppauge, NY, USA). After that, the sample was electroporated in an E2510 electroporator (Eppendorf, Hauppauge) with three pulses at 0–2000 V, and stored at 4 °C for 5 min. Unbound NORAD was removed by rinsing with PBS. EVs with FITC-NORAD (green) were labeled with Dil (red) and incubated with osteosarcoma cells for 48 h. Finally, the co-localization of FITC and Dil in the recipient cells was observed under a fluorescence microscope (ECLIPSE E800, Nikon, Japan).

### Reverse transcription-quantitative polymerase chain reaction (RT-qPCR)

Total RNA content (500 ng) was extracted using Takara Prime Script RT master mix kits (Takara, Cat No. RR037B), and reverse-transcribed to complementary DNA (cDNA) with TaqMan MicroRNA Reverse Transcription kits (4366596, Thermo Fisher Scientific). Next, RT-qPCR was performed to detect the mRNA expression patterns using SYBR Premix Ex Taq II kits (Takara, Cat No. 2). All mRNA primers used in this study are listed in Table S2. TaqMan probes were purchased from Thermo Fisher Scientific (Cat No. 1). Glyceraldehyde-3-phosphate dehydrogenase (GAPDH) and U6 were regarded as the internal reference gene of NORAD and miRNA, respectively. When measuring the expression patterns of NORAD in EVs, an endogenous reference of 0.1 ng ( $1.8 \times 10^8$  copies) λpolyA + RNA (Takara) synthesis was added at the beginning of RNA reverse transcription to normalize total RNA in EVs. The calculation of each sample was performed by means of relative quantification (the  $2^{-\Delta\Delta C_t}$  method).

### Dual luciferase reporter gene assay

The NORAD sequence containing miR-30c-5p binding site and its mutant sequence were cloned into pGL3-Promoter Luciferase reporter vector (Promega, Madison, WI, USA) to construct the wild-type (WT)-NORAD and mutant (MUT)-NORAD reporter vectors. HEK-293T cells were then co-transfected with miR-30c-5p mimic and the above report vector using Lipofectamine 2000 (Invitrogen). After 24 h, the supernatant of HEK-293T cells was collected. Luciferase activity was subsequently measured using a dual luciferase reporter system (E1910, Promega). The relative luciferase activity was determined as Firefly luciferase divided by Renilla luciferase. The same method was used to detect the binding ability of miR-30c-5p to KLF10. miR-30c-5p mimic and pGL3-Luciferase Reporter vector (Promega) containing WT KLF10-3' untranslated region (3'UTR) or MUT KLF10-3'UTR were transfected into HEK293T cells. Each experiment was repeated 3 times to obtain the mean value.

The NORAD cDNA sequences containing potential miRNA binding sites and mutant miRNA binding site were cloned into the mammalian expression vector pcDNA3.1 (Invitrogen). Subsequently, WT-KLF10, MUT-KLF10, pcDNA3.1, pcDNA3.1-NORAD, pcDNA3.1-NORAD-MUT, pcDNA3.1 NORAD + miR-30c-5p mimic, or miR-30c-5p mimic were transfected into 143B cells using lipofectamine 2000. The relative luciferase activity was calculated after 48 h of transfection.

### RNA immunoprecipitation (RIP)

RIP was performed using the Magna-RNA binding protein immunoprecipitation kits (Millipore, Billerica, MA, USA) according to the manufacturer's instructions. Briefly, the entire cell lysate was added with normal mouse immunoglobulin G (IgG) as NC or RIP buffer containing human-derived anti-Argonaute 2-conjugated magnetic beads, and incubated with proteinase K. The RNA concentration was then detected using a spectrophotometer (Thermo Fisher Scientific), and the RNA quality was assessed using a bio-analyzer (Agilent, Santa Clara, CA, USA). Finally, RNA content was extracted and the purified RNA was detected using RT-qPCR to verify the presence of binding sites.

### RNA pull-down assay

First, osteosarcoma cells were transfected with biotin-labeled WT-NORAD and biotin-labeled MUT-NORAD (50 nM each). After 48 h of transfection, the cells were collected and incubated with cell lysate (Ambion, Austin, Texas, USA) for 10 min. Afterwards, 50 mL of cell lysate sample was aliquoted. Next, the residual lysate was incubated with M-280 streptavidin magnetic beads (Sigma) pre-coated with RNase-free and yeast tRNA (Sigma) at 4 °C for 3 h. The mixture was then washed twice with cold lysate, three times with low-salt buffer, and once with high-salt buffer. Finally, RNA content was extracted for RT-qPCR detection.

### Fluorescence in situ hybridization (FISH)

When cell confluence reached 60–70%, the cells were fixed with 4% formaldehyde for 10 min, and permeated in 0.5% TritonX-100 at 4 °C for 15 min. The FITC-labeled NORAD cell probe was incubated overnight at 37 °C, and then rinsed with  $2 \times$  saline sodium citrate (SSC) 6 times for 3 min. Next, Cy3-labeled miR-30c-5p probe and pre-hybridization buffer (1:100) were incubated at 88 °C for 3–5 min. Following incubation, the cells were incubated with Cy3-labeled miR-30c-5p probe overnight at 37 °C, washed 6 times with  $2 \times$  SSC for 3 min, and washed 3 times with  $2 \times$  SSC for 5 min. Finally, the cells were observed under a fluorescence microscope (Olympus, Tokyo, Japan) with five random fields.

### Transwell assay

First, 50 µL Matrigel (Sigma) was spread in the chamber before the experiment. Osteosarcoma cells at the logarithmic phase of growth were starved for 24 h, and detached the following day to make the final concentration of  $2 \times 10^5$ /mL. The upper chamber of Transwell was added with 0.2 mL of the suspension, while the lower chamber was added with 700 µL DMEM containing 10% FBS for incubation in an incubator at 37 °C with 5% CO<sub>2</sub>. After 24 h, the cells were removed from the Transwell chamber, fixed with methanol, and stained with 0.1% crystal violet. Five fields were then randomly selected under an inverted microscope (XDS-800D, Shanghai Caikang Optical Instrument Co., Ltd., Shanghai, China), and the number of stained cells was counted and expressed as an average. For EV treatment, osteosarcoma cells were seeded in 6-well plates. After 24 h, new medium was replaced and added with EVs or an equal amount of PBS.

### Cell counting kit-8 (CCK-8) assay

Cells were incubated with a CCK-8 solution (10 µL, Dojindo, Japan) in 96-well plates at 37 °C for 1–3 days. A microplate reader (Thermo Fisher Scientific) was used to measure the absorbance at a wavelength of 450 nm.

### Western blot analysis

Total protein content was extracted from tissues and cells using RIPA lysis buffer (R0010, Beijing Solarbio Science & Technology Co. Ltd., Beijing, China). The obtained protein was lysed for 15 min at 4 °C and centrifuged at  $12,000 \times g$  for 15 min with the supernatant collected for protein concentration determination with BCA kits (23227, Thermo Fisher Scientific). The proteins were then separated by sodium dodecyl sulfate-polyacrylamide gel electrophoresis, and transferred to the polyvinylidene fluoride membrane. The membrane was blocked with 5% bovine serum albumin for 1 h at room temperature and incubated overnight at 4 °C with diluted rabbit primary antibodies, including KLF10 (dilution ratio of 1:1000, ab73537), and GAPDH (dilution ratio of 1:10,000, ab8245, Abcam). After 3 times washes with TBST (each for 5 min), the membrane was incubated with the horseradish peroxidase-labeled goat anti-rabbit IgG (dilution ratio of 1:20,000, ab205718, Abcam) at room temperature for 1 h. The membrane was then developed, and semi-quantification of the bands was performed using the Image J 1.48 software (National Institutes of Health) and normalized to GAPDH. The experiment was repeated three times to obtain the mean value.

### Xenograft tumor model and lung metastasis model

Specific pathogen free immunodeficient nude mice (aged 4–5 week old, BALB/c, nu/nu, Liaoning Changsheng Biotechnology Co., Ltd., Benxi, Liaoning, China) were housed under an environment of 26–28 °C and 50–65% humidity. According to previous studies [25, 26], 143B osteosarcoma cell line exhibits a high rate of subcutaneous tumor formation or lung metastasis, thus, we selected the 143B osteosarcoma cell line to construct xenograft tumor models. The concentration of 143B osteosarcoma cells was adjusted to  $2 \times 10^7$  cells/mL, and 143B cells were then injected subcutaneously in the back of nude mice. Trypan blue elimination determined that 95 percent of the cells were viable prior to injection. Eight days after injection, nude mice were treated with PBS, BMSC-EVs (10 µg EVs isolated from BMSCs), BMSC-EV-shNC (EVs isolated from shNC lentivirus-infected BMSCs), or BMSC-EV-shNORAD (EVs isolated from shNORAD lentivirus-infected BMSCs), respectively ( $n = 10$ ). Next, the tumor volume was measured every 4 days:  $W = 1/2 \times a \times b^2$  ( $a$ , long diameter;  $b$ , short diameter). Three weeks later, the mice were sacrificed by CO<sub>2</sub>, and the tumor tissue was stripped and weighed.

For the lung metastasis model, the 143B cells stably-treated with pcDNA NORAD and sh-NORAD were injected into the female BALB/c nude mice

via the tail vein. After 7 weeks of treatment, all mice were sacrificed and the number of lung metastatic nodules and lung weight were evaluated. Meanwhile, for BMSC-EVs treatment, 143B osteosarcoma cells were injected into the tail vein to develop lung metastasis. Fourteen days after injection, the mice were divided into 4 groups (10 mice per group) according to the equivalent range of tumor size. Next, the mice were repeatedly injected with 10  $\mu$ g of EVs or PBS via the tail vein twice a week for a month. After 7 weeks of tumor growth, all mice were sacrificed, and the number of lung metastatic nodules and lung weight were evaluated. The expression patterns of NORAD and miR-30c-5p in lung tissues from bone marrow sample were detected, and the lungs were isolated for Western blot detection and hematoxylin-eosin (HE) staining.

### HE staining

HE staining was used to detect the effect of NORAD on the metastasis of osteosarcoma. The removed lung tissue block was fixed with fixative solution (10% formalin, Bouin's fixative solution, etc.), rinsed with water for 30 min, dehydrated with alcohol at different concentrations, incubated with xylene, embedded in wax, sectioned, dewaxed and stained.

### Bioinformatics analysis

The osteosarcoma GSE70414 dataset comprising of 1 normal sample and 5 osteosarcoma samples was obtained from the Gene Expression Omnibus database (GEO); (<https://www.ncbi.nlm.nih.gov/geo/>). Differentially analysis was subsequently performed using the R language "limma" package with threshold set as  $|\log_2\text{FoldChange}| > 1$  and  $p < 0.05$  as the screening standard. In addition, the target gene of miR-30c-5p was predicted using the miRDIIP database (<http://ophid.utoronto.ca/mirDIP/index.jsp#r>), TargetScan database ([http://www.targetscan.org/vert\\_71/](http://www.targetscan.org/vert_71/)) and miRDB database (<http://mirdb.org/>). Meanwhile, the candidate target genes were analyzed for interaction analysis, and other genes that might interact with miR-30c-5p were predicted using the GeneMANIA database (<http://genemania.org/>).

### Statistical analysis

Statistical analyses were performed using the GraphPad Prism 8.0 software (GraphPad Software, La Jolla, CA, USA), and all experiments were repeated at least 3 times independently. Measurement data were expressed as mean  $\pm$  standard deviation. Comparisons between cancer tissues and adjacent tissues were examined by paired *t* test, while comparisons between other two groups were examined by unpaired *t* test. Comparisons of multiple groups of data were examined by one-way analysis of variance (ANOVA), followed by Tukey's post-hoc test. Two-way ANOVA or repeated measures ANOVA was performed for comparisons between groups at multiple time points, followed by Tukey's post-hoc test. Survival analysis was performed using Kaplan–Meier method and tested with log-rank test. Spearman's rank correlation coefficient was employed for correlation analysis between miR-30c-5p and NORAD as well as between NORAD and KLF10 in osteosarcoma tissues. A value of  $p < 0.05$  was regarded statistically significant.

## RESULTS

### Highly-expressed NORAD was associated with lung metastasis of osteosarcoma

A previous study has shown that NORAD regulates the proliferation and migration of osteosarcoma cells [22]. In order to further understand the role of NORAD in osteosarcoma, we performed RT-qPCR for quantification of lncRNA NORAD, and found that NORAD expression levels were increased in osteosarcoma tissues and metastatic osteosarcoma tissues relative to normal tissues, while higher NORAD expression was detected in metastatic osteosarcoma tissues than that in osteosarcoma tissues (Fig. 1A, B). The Kaplan–Meier curve further indicated that the survival of patients with low NORAD expression was longer than that of patients with high NORAD expression (Fig. 1C). In addition, we assigned 30 patients into 2 groups ( $n = 15$ ) based on the median value of NORAD expression. As shown in Table A1, NORAD was not significantly correlated with gender, age or tumor site yet significantly correlated with Enneking classification, differentiation and metastasis. In addition, the aforementioned increased NORAD expression levels were confirmed in 4 different osteosarcoma cell

lines in comparison to hFOB 1.19 cell line (Fig. 1D). In addition, we established an in vivo lung metastasis models in order to investigate the effect of NORAD on lung metastasis of osteosarcoma. The osteosarcoma 143B cells were infected with lentivirus expressing sh-NORAD (Lv-sh-NORAD) or lentivirus overexpressing NORAD (Lv-NORAD), and the results of RT-qPCR confirmed that Lv-sh-NORAD infection effectively down-regulated the NORAD expression, while Lv-NORAD upregulated the NORAD expression (Fig. 1E). Moreover, in vivo osteosarcoma metastasis model results showed that following injection of 143B cells infected with Lv-NORAD in mice, lung metastatic nodules and lung weight exhibited an increase, while injection of 143B cells infected with sh-NORAD lentivirus caused suppression of lung metastasis (Fig. 1F–I). These results suggested that highly-expressed NORAD was correlated with poor prognosis, and further promoted lung metastasis of osteosarcoma.

### BMSC-EVs transported NORAD into osteosarcoma cells

Osteosarcoma cells stimulated by BMSCs possess an enhanced ability to migrate across endothelial cells [27]. In order to investigate whether BMSCs could transfer NORAD into osteosarcoma cells, we isolated and purified BMSCs from bone marrow. Observation under an optical microscope illustrated that BMSCs were spindle-shaped, growing in colonies, arranged like a vortex when dense, as shown in Fig. S1A. In addition, BMSCs exhibited osteogenic, adipogenic, and chondrogenic differentiation function (Fig. S1B). The BMSC-EVs were further isolated from conditioned supernatant, and analyzed by means of TEM and NTA, which revealed that the isolated particles exhibited double-layer membrane with diameter ranged 30–120 nm (Fig. 2A, B). According to Western blot assay, positive expression of Alix, TSG101, and CD81 was detected in EVs, while non-EVs markers such as GRP94 and plasma lipoproteins such as APOB were found to be negative (Fig. 2C). These findings suggested that the EVs were successfully isolated from BMSCs.

To further explore the effect of BMSC-EVs on osteosarcoma cells, we co-cultured PKH67-labeled BMSC-EVs or PBS with osteosarcoma cells for 12 h (Fig. 2D). As a sequence, it was observed that a large number of BMSC-EVs were distributed in osteosarcoma cells around the nucleus, while osteosarcoma cells treated with PBS did not exhibit green fluorescence. Meanwhile, the EVsrbase website (<http://www.EVsrbase.org>) indicated that NORAD was present in circulating EVs and a variety of cells. Therefore, we then explored the existence of NORAD in BMSC-EVs. To evaluate whether NORAD was encapsulated in EVs or on the surface of EVs, RNase protection assay was performed on the EVs in the medium. Following treatment with detergent to destroy the vesicle membrane, EVs were incubated with RIPA buffer for 20 min, with RNase A, and then with lysis buffer. It was found that following treatment with only RNase, NORAD level in the medium did not change, whereas the additional application of Triton X100, a detergent to dissolve lipid, brought about a reduction in the level of NORAD (Fig. 2E). The above-mentioned findings demonstrated that NORAD was enveloped by the membrane rather than being directly released. In order to further explore the transfer of NORAD, FITC-NORAD (green) was electrically transfected to BMSCs, followed by the extraction of EVs. The EVs were labeled with Dil (red) and incubated with osteosarcoma cells for 48 h. The co-localization of FITC and Dil was observed in recipient osteosarcoma cells under a microscope, and it was found that the osteosarcoma cells internalized the EVs containing FITC-NORAD (Fig. 2F). Moreover, the expression of NORAD in osteosarcoma cells was increased after co-culture with BMSC-EVs, while showing no significant changes following co-culture with EV-depleted BMSC medium (Fig. 2G). These findings supported that NORAD in BMSCs could be transported to osteosarcoma cells through EVs.

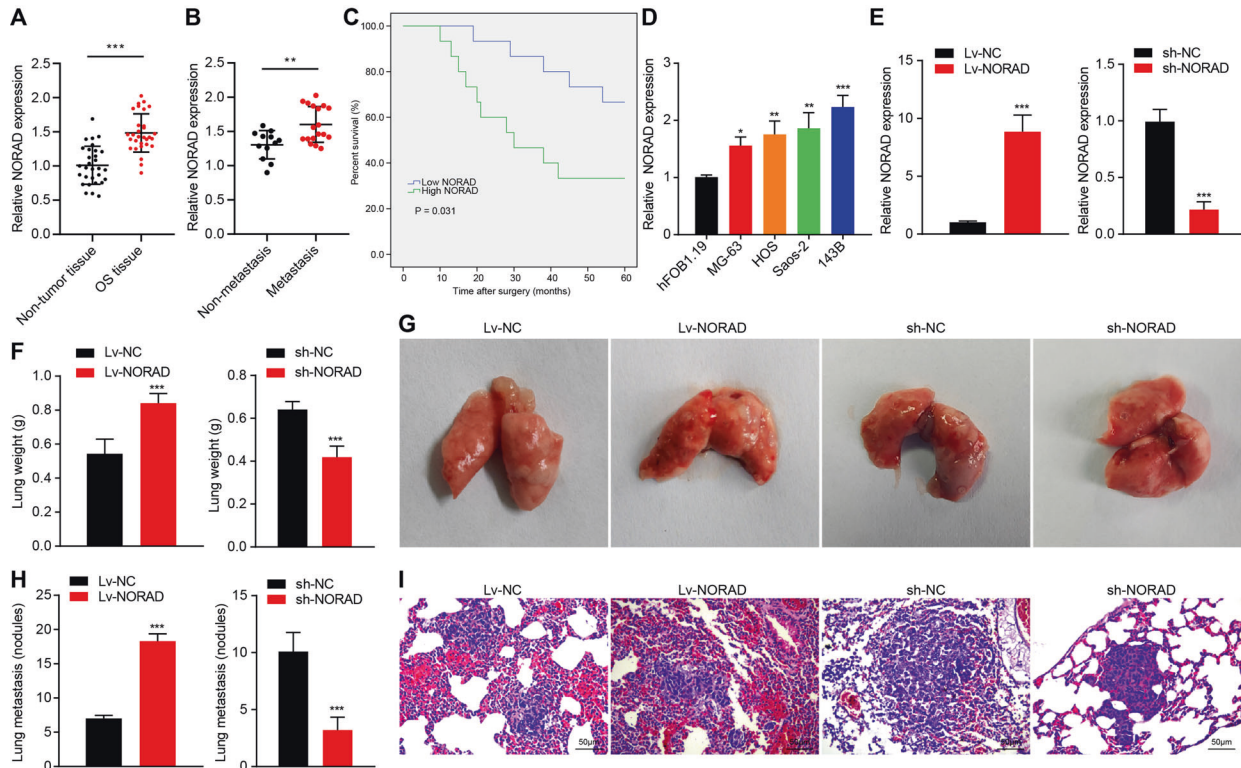


**Fig. 1 NORAD induced lung metastasis of osteosarcoma.** **A** Detection of NORAD expression in osteosarcoma tissues and adjacent tissues by RT-qPCR ( $n = 30$ ). **B** Detection of NORAD expression in metastatic osteosarcoma tissues ( $n = 18$ ) and non-metastatic osteosarcoma tissues by RT-qPCR ( $n = 12$ ). **C** Kaplan–Meier survival curve analysis of the correlation between NORAD expression and overall survival. **D** Detection of NORAD expression in human osteoblast hFOB 1.19 and osteosarcoma cell lines 143B, HOS, Saos-2, and MG-63 by RT-qPCR. **E**, The expression of NORAD in 143B cells was detected by RT-qPCR after knocking down or overexpressing NORAD. **F** Nude mice were injected with NORAD-deficient or NORAD-overexpressed osteosarcoma cells ( $n = 10$ ), sacrificed 7 weeks later, and assessed for lung weight. **G** Representative image of metastatic lung tissues ( $n = 10$ ) upon treatment with knocking down or overexpressing NORAD. **H** The number of lung metastatic nodules from mice injected with 143B cells treated with Lv-NORAD, sh-NORAD, or controls. ( $n = 10$ ). **I**, HE staining showing metastatic lung nodules (scale bar = 50  $\mu\text{m}$ ;  $n = 10$ ). The measurement data were expressed as mean  $\pm$  standard deviation, the comparison between cancer tissues and adjacent tissues were examined by paired  $t$  test, the comparison between other two groups were examined by unpaired  $t$  test, and the comparison of multiple groups of data were examined by one-way ANOVA, followed by Tukey's post hoc test. \* $p < 0.05$ , \*\* $p < 0.01$ , \*\*\* $p < 0.001$  vs. adjacent tissues, hFOB 1.19 cells, cells with Lv-NC or sh-NC. The experiment is repeated at least 3 times independently.

### NORAD derived from BMSC-EVs promoted proliferation and invasion of osteosarcoma cell

To investigate the effect of NORAD derived from BMSC-EVs on osteosarcoma cell metastasis, we knocked NORAD down in BMSCs to observe the changes in cells. The results of RT-qPCR demonstrated that NORAD expression levels in BMSCs and the extracted MSC-EVs were effectively reduced after NORAD knockdown (Fig. 3A). Subsequently, osteosarcoma cells were incubated with the extracted MSC-EVs or BMSCs, and RT-qPCR findings revealed that the expression of NORAD in osteosarcoma cells incubated with MSC-EVs were increased, while exhibiting no significant changes in osteosarcoma cells upon incubation with BMSC-EV-shNORAD (Fig. 3B). In addition, the proliferation and invasion abilities of recipient osteosarcoma cells incubated with MSC-EVs were found to be improved, while down-regulation of NORAD in BMSC-EVs reduced the malignant capacities of osteosarcoma cells (Fig. 3C, D). These results indicated that BMSC-EVs-NORAD promoted the proliferation and invasion of osteosarcoma cells.

### NORAD induced the proliferation and invasion of osteosarcoma cells by sponging miR-30c-5p

In addition, miR-30c-5p has been recently reported in a ceRNA network to play a role in the occurrence of osteosarcoma [21]. Bioinformatic analysis performed using the StarBase website (<http://starbase.sysu.edu.cn/>) suggested the presence of binding sites between NORAD and miR-30c-5p (Fig. 4A). Subsequently, we

mutated the miR-30c-5p binding site, and the luciferase report assay showed that miR-30c-5p mimic inhibited the luciferase activity of WT-NORAD, but did not affect that of MUT-NORAD (Fig. 4B). In addition, FISH results showed that NORAD and miR-30c-5p were co-localized in the 143B cells (Fig. 4C). Moreover, a strong interaction was observed between miR-30c-5p and NORAD, as demonstrated by RIP assay, suggesting the presence of NORAD in miR-30c-5p RNA-induced silencing complex (Fig. 4D). The results of RNA pull-down assay demonstrated that the lysate of WT-NORAD- or MUT-NORAD-treated osteosarcoma cells bound to beads, where RT-qPCR demonstrated high content of miR-30c-5p in the pull-down pellets by NORAD-WT (Fig. 4E), indicating the specific recognition of miR-30c-5p on NORAD. We further examined the levels of miR-30c-5p in clinical samples, which revealed that the expression of miR-30c-5p in OS tissues was negatively correlated with the expression of NORAD (Fig. 4F). Together, these results proved that miR-30c-5p can be competitively bound by NORAD.

To further explore whether interaction of NORAD and miR-30c-5p influenced the malignant capacities of osteosarcoma cells, we treated MG-63 osteosarcoma cells with Lv-NORAD and miR-30c-5p mimic, whilst 143B cells were treated with Lv-sh-NORAD and miR-30c-5p inhibitor. Subsequent results demonstrated that over-expression of NORAD diminished the levels of miR-30c-5p and improved the proliferation and invasion of MG-63 cells, while miR-30c-5p mimic reversed the pro-proliferative and pro-invasive

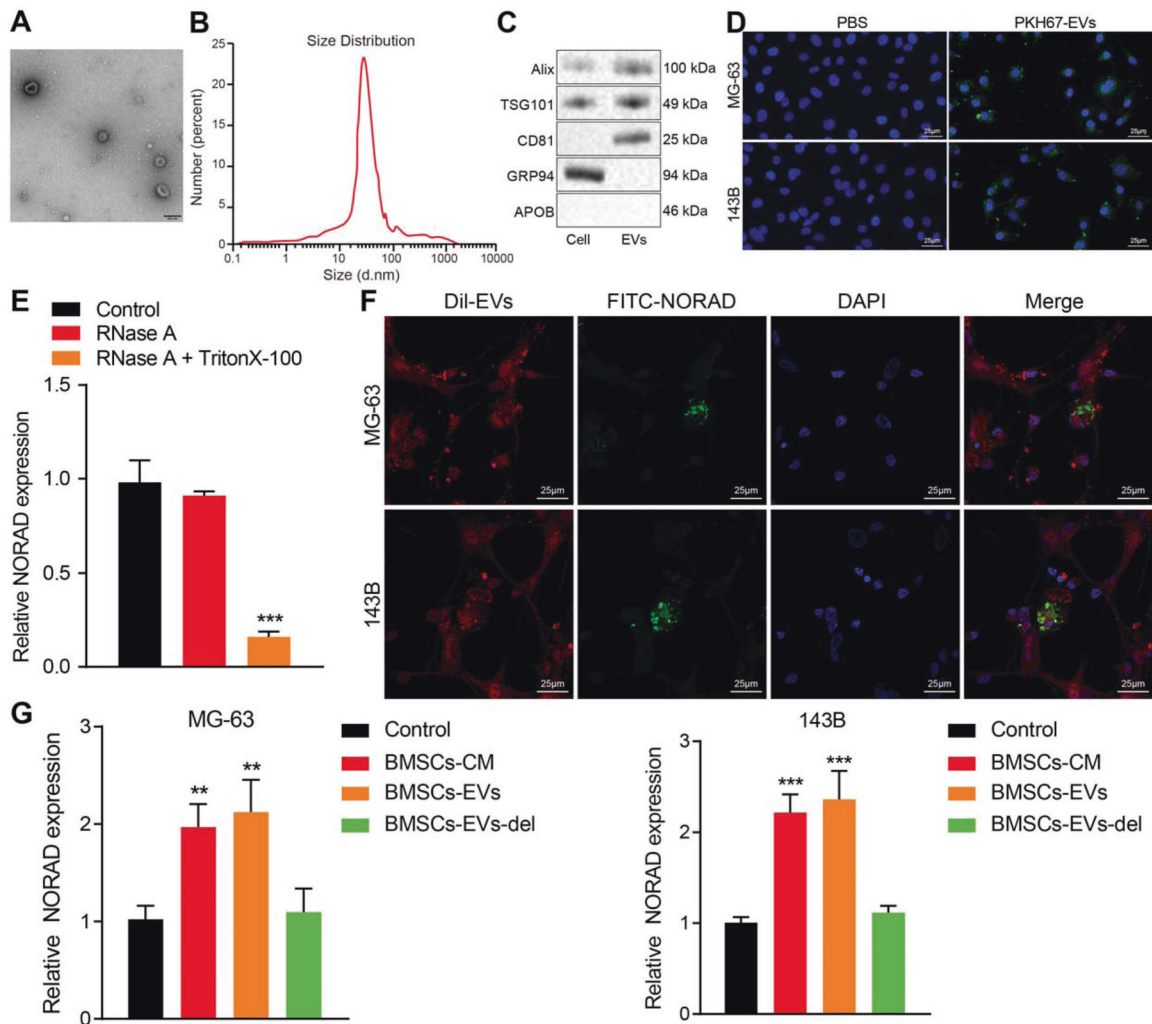


**Fig. 2** BMSC-EVs transmitted NORAD to osteosarcoma cells. **A** Representative TEM images of morphology of EVs. Scale bar = 100 nm. **B** Detection of EV diameter and concentration by NTA. **C** Western blot analysis showing the expression of EV markers Alix, TSG101, CD81, endoplasmic reticulum protein GRP94 and plasma lipoprotein APOB. **D** Immunofluorescence microscopy was used to observe the internalization of BMSC-EVs labeled with PKH67 (green) by osteosarcoma cells. Nucleus stained with DAPI (blue). Scale bar = 25  $\mu$ m. **E** RT-qPCR showing the expression of NORAD in EVs treated with RNase and detergent. **F** The co-localization of FITC-NORAD (green) and Dil-EVs (red) in osteosarcoma cells, with nuclei stained with DAPI (blue). Scale bar = 25  $\mu$ m. **G** RT-qPCR showing the expression of NORAD in osteosarcoma cells co-cultured with BMSC-EVs. The measurement data were expressed as mean  $\pm$  standard deviation. The comparison of multiple groups of data was analyzed by one-way ANOVA, followed by Tukey's post hoc test. \* $p$  < 0.05, \*\* $p$  < 0.01, \*\*\* $p$  < 0.001 vs. control. The experiment was repeated at least 3 times independently.

effects of NORAD (Fig. 4G–I). Meanwhile, NORAD knockdown elevated the miR-30c-5p levels and impeded the proliferation and invasion of 143B cells, both of which were rescued after inhibition of miR-30c-5p. The above results indicated that NORAD can competitively bind to miR-30c-5p and promote the proliferation and invasion of osteosarcoma cells.

#### NORAD upregulated KLF10 by sponging miR-30c-5p

After uncovering the regulation of miR-30c-5p by NORAD in osteosarcoma cells, we speculated whether NORAD may regulate the target gene of miR-30c-5p by acting as a ceRNA. To explore the target genes of miR-30c-5p, the GSE70414 dataset was retrieved from the GEO database. Subsequent analysis of the dataset revealed that 79 genes were significantly highly expressed in osteosarcoma (Fig. S2). In addition, target genes of miR-30c-5p were predicted using the miRDIIP, TargetScan, and miRDB database, while 8 genes were found at the intersection of the predicted target genes and up-regulated genes (Fig. S3). Next, these 8 genes and other related genes were included to construct

a gene-gene interaction map (Fig. 5A). It was found that the KLF10 gene was the hub gene (Table S3), indicating that KLF10 might play a key modulatory role in the disorder. The binding sites of miR-30c-5p and KLF10 were obtained through StarBase website. To further verify whether miR-30c-5p reduced the expression of KLF10 by binding to its 3'UTR, we designed sequences of WT-KLF10 and MUT-KLF10 and performed a dual luciferase reporter gene assay. It was found that miR-30c-5p mimic decreased the luciferase activity of WT-KLF10, but did not affect the luciferase activity of MUT-KLF10 (Fig. 5B). Next, a WT/MUT KLF10 3'UTR luciferase reporter was constructed in 143B cells transfected with pcDNA-NORAD/pcDNA-NORAD mut. Over-expression of pcDNA-NORAD, rather than pcDNA-NORAD mut, increased the luciferase activity of pmirGLO-KLF10 luciferase reporter, while miR-30c-5p mimic was found to counter this effect (Fig. 5C). Meanwhile, the results of Spearman correlation analysis showed that NORAD levels in osteosarcoma tissues were positively correlated with KLF10 expression (Fig. 5D). Then, 143B and MG-63 cells were treated with miR-30c-5p mimic or inhibitor, and it was observed

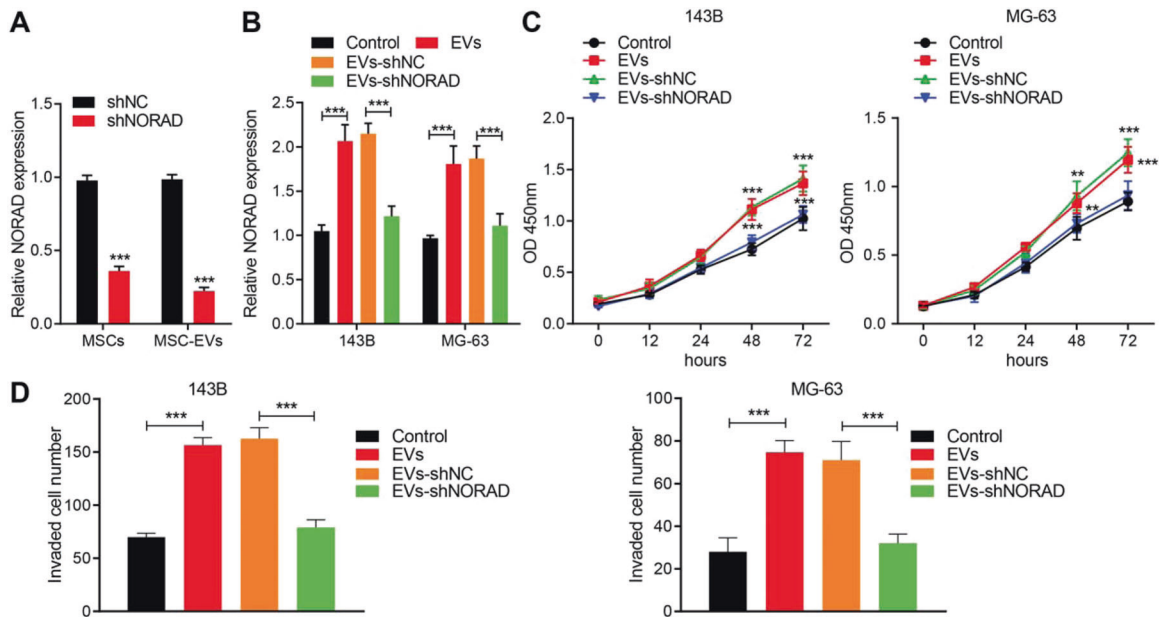


**Fig. 3 NORAD in BMSC-EVs enhanced the proliferative and invasive potentials of osteosarcoma cells.** **A** RT-qPCR showing NORAD expression in BMSCs and BMSC-EVs after NORAD knockdown. **B** RT-qPCR showing NORAD expression in osteosarcoma cells cultured with BMSC-EVs. **C** Proliferation of osteosarcoma cells cultured with BMSC-EVs, BMSC-shNORAD or controls detected by CCK-8. **D** The invasion of osteosarcoma cells cultured with BMSC-EVs, BMSC-shNORAD or controls were detected by Transwell assay. The measurement data were expressed as mean  $\pm$  standard deviation. The comparison between two groups was examined by unpaired *t*-test, and the comparison of multiple groups of data was examined by one-way ANOVA. Two-way ANOVA was used for comparison between groups at multiple time points, followed by Tukey's post hoc test. \**p* < 0.05, \*\**p* < 0.01, \*\*\**p* < 0.001 vs. shNC, Control, or EVs-shNC. The experiment was repeated at least 3 times independently.

that treatment with miR-30c-5p mimic reduced KLF10 levels, while miR-30c-5p inhibitor enhanced KLF10 levels (Fig. 5E). To further explore whether NORAD regulated KLF10 through miR-30c-5p, 143B cells were treated with Lv-NORAD alone or in combination with miR-30c-5p mimic, and MG-63 cells were treated with sh-NORAD or miR-30c-5p in combination with miR-30c-5p inhibitor, respectively. The results demonstrated MG-63 cells exhibited increased KLF10 levels after NORAD over-expression, while miR-30c-5p mimic countered this effect; 143B cells exhibited decreased KLF10 levels after NORAD knockdown, while treatment with miR-30c-5p inhibitor rescued the KLF10 expression (Fig. 5F). These data suggested that NORAD may serve as a ceRNA of miR-30c-5p, leading to increased expression of KLF10.

#### EV-NORAD up-regulated miR-30c-5p-mediated KLF10 to promote the proliferation and invasion of osteosarcoma cells

We then set out to investigate whether the BMSC-EV-NORAD could up-regulate the expression of KLF10. The results of RT-qPCR demonstrated that miR-30c-5p levels were reduced in osteosarcoma cells co-cultured with BMSC-EVs, while being up-regulated after osteosarcoma cells were incubated with BMSC-EV-shNORAD (Fig. 6A). It was also found that treatment with sh-KLF10 effectively decreased the KLF10 expression in 143B cells or MG-63 cells, whereas incubation with BMSC-EVs could partially restore KLF10 levels, while treatment with BMSC-EV-shNORAD brought about lower KLF10 levels compared to treatment with BMSC-EVs (Fig. 6B). Furthermore, the proliferation and invasion of osteosarcoma cells were observed to be significantly reduced following KLF10 knockdown, and both of which could be rescued after the cells were incubated with BMSC-EVs, while BMSC-EV-shNORAD led to suppressed cell proliferation and invasion compared to treatment with BMSC-EVs (Fig. 6C, D). The above results indicated that EVs derived from BMSCs could deliver NORAD to osteosarcoma cells to mediate the miR-30c-5p/KLF10 axis, whereby accelerating the proliferation and invasion of osteosarcoma cells.

#### BMSC-EV-NORAD promoted lung metastasis of osteosarcoma

Last, to observe the effect of BMSC-EVs on the tumor formation, subcutaneous xenograft models were constructed. After injection with BMSC-EVs, the volume and weight of the transplanted tumors were found to be increased, but injection with BMSC-EV-shNORAD brought about reductions in tumor volume and weight as compared to injection with BMSC-EVs (Fig. 7A–C). In order to further investigate the effect of BMSC-EV-NORAD on lung metastasis of osteosarcoma, we injected 143B cells into nude mice through the tail vein. After 2 weeks, BMSC-EVs or equal amounts of PBS were injected into the tail vein of mice, twice a week for a duration of 1 month. It was observed that the lung weight and metastatic pulmonary nodules were significantly increased in mice injected with BMSC-EVs, but BMSC-EV-shNORAD led to reduced lung weight, and metastatic pulmonary nodules compared to treatment with BMSC-EVs (Fig. 7D–G). As for the expression patterns of NORAD, miR-30c-5p, and KLF10 in the lung tissues, the results of RT-qPCR and Western blot analyses demonstrated increased levels of NORAD and KLF10, and decreased miR-30c-5p in the lung tissues of mice injected with BMSC-EVs, whereas mice injected with BMSC-EV-shNORAD exhibited lower NORAD/KLF10 and higher miR-30c-5p expression in the lung tissues compared to mice injected with BMSC-EVs (Fig. 7H, I). The above results suggested that NORAD from BMSC-EVs upregulated KLF10 via miR-30c-5p, thereby promoting lung metastasis of osteosarcoma.

#### DISCUSSION

As the chief component of TME, mesenchymal stem cells are present in a plethora of tissues, such as adipose tissues, bone marrow, umbilical cord and placenta [28]. Meanwhile, BMSC-conditioned medium can promote the growth and migration of osteosarcoma cells [29]. Based on our data, we further found that BMSC-derived EVs play a key role in regulating tumor cell

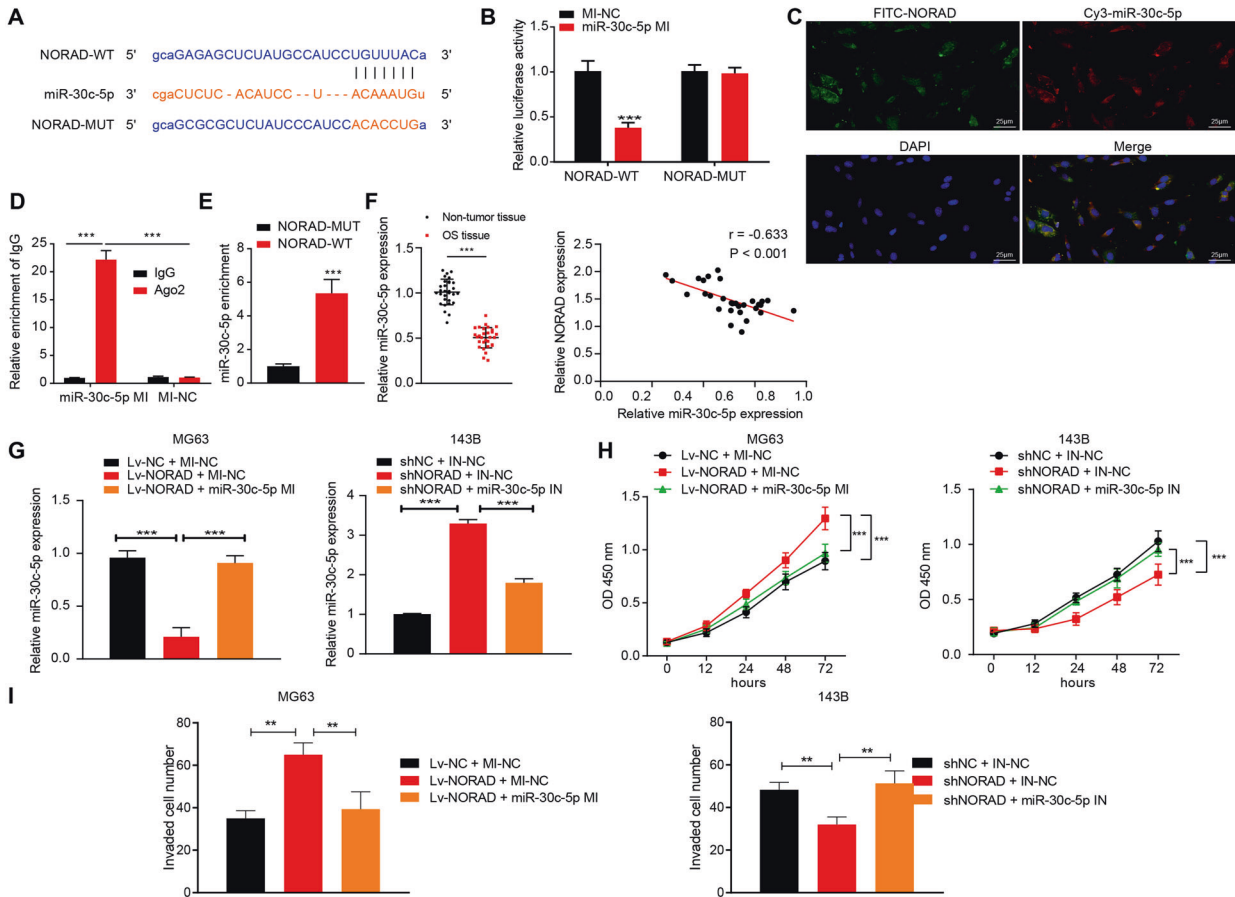


**Fig. 4** NORAD adsorbing miR-30c-5p affected the proliferation and invasion of osteosarcoma cells. **A** The binding site and mutation site between NORAD and miR-30c-5p. **B** Dual luciferase reporter assay was used to detect the luciferase activity of WT/MUT-NORAD in HEK-293T cells. \*\*\* $p < 0.001$  vs. mimic (MI)-NC. **C** FISH showing the colocalization of Cy3-miR-30c-5p (red) and FITC-NORAD (green) in 143B cells. Scale bar = 25  $\mu$ m; DAPI, blue. **D** The relationship between NORAD and miR-30c-5p was detected by RIP after HEK-293T cells were transfected with miR-30c-5p mimic or mimic-NC. \*\*\* $p < 0.001$  vs. IgG. **E**, RT-qPCR showing the enrichment of miR-30c-5p pulled down by biotinylated NORAD and NC probes. \*\*\* $p < 0.001$  vs. MUT-NORAD. **F** RT-qPCR showing the relative expression of miR-30c-5p in osteosarcoma tissues and adjacent tissues (left) and Spearman correlation showing the correlation between NORAD level and miR-30c-5p expression in osteosarcoma tissues (right) ( $n = 30$ ). **G** RT-qPCR showing the expression of miR-30c-5p after transfection of NORAD overexpression plasmid or miR-30c-5p mimic in osteosarcoma cells. **H** CCK-8 was used to detect the proliferation of osteosarcoma cells after transfection of NORAD overexpression plasmid or miR-30c-5p mimic in osteosarcoma cells. **I** Transwell assay was used to detect the invasion of osteosarcoma cells after transfection of NORAD overexpression plasmid or miR-30c-5p mimic in osteosarcoma cells. The measurement data were expressed as mean  $\pm$  standard deviation. The comparison between cancer tissues and adjacent tissues were examined by paired  $t$  test. The comparison between other two groups was examined by unpaired  $t$  test, and the comparison of multiple groups of data was examined by one-way ANOVA. Repeated measures ANOVA was used for comparison between groups at multiple time points, followed by Tukey's post hoc test. The experiment was repeated at least 3 times independently.

proliferation and invasion. In this study, we clarified that highly expressed NORAD promoted lung metastasis of osteosarcoma. BMSC-EVs delivered NORAD to osteosarcoma cells to regulate miR-30c-5p/KLF10 axis, thereby promoting proliferation, invasion, and lung metastasis of osteosarcoma cells (Fig. 8).

TME serves as the playground for numerous interactions, including the communication between tumor cells and other cells [30]. In addition, BMSCs possess the ability to regulate certain pathways in osteosarcoma cells to enhance their lung metastasis [31]. BMSCs are further used for cell transplantation therapy due to their multi-directional differentiation potential, no immunogenicity, and other advantages [32]. Previous studies have also highlighted the enhanced migration of osteosarcoma across the endothelium upon stimulation by BMSCs and capillary network of endothelial cells [27]. This particular phenomenon of cell-to-cell communication can possibly be attributed to EVs. Inherently, EVs are nano-vesicles that are secreted by the greater part of cell types in the body [33], including BMSCs. Expanding on our current knowledge, findings obtained in our study demonstrated that the

vesicles isolated from BMSC conditioned media were double-membraned vesicles in the range of 30–120 nm. A growing number of studies have further shown that BMSC-derived EVs, by modulating the RNA/protein expression in recipient cells, promote or inhibit tumor growth, highlighting them as potential targets for clinical applications [34, 35]. Our findings revealed that BMSC-EVs carried the lncRNA NORAD into osteosarcoma cells and promoted tumor progression.

Furthermore, a large number of studies have documented the involvement of non-coding RNAs, especially miRNA and lncRNA in various biological and pathological processes occurring during the course of osteosarcoma development [36–38]. A newly-identified lncRNA, NORAD is known to be highly-conserved, abundantly expressed in several malignancies, and maintains chromosome stability [18]. In the current study, we documented up-regulated levels of NORAD in both osteosarcoma cells and osteosarcoma tissues. Also, recent evidence has also illustrated transfection of osteosarcoma cell Saos-2 and 143B cells with NORAD-specific small interfering RNAs brought



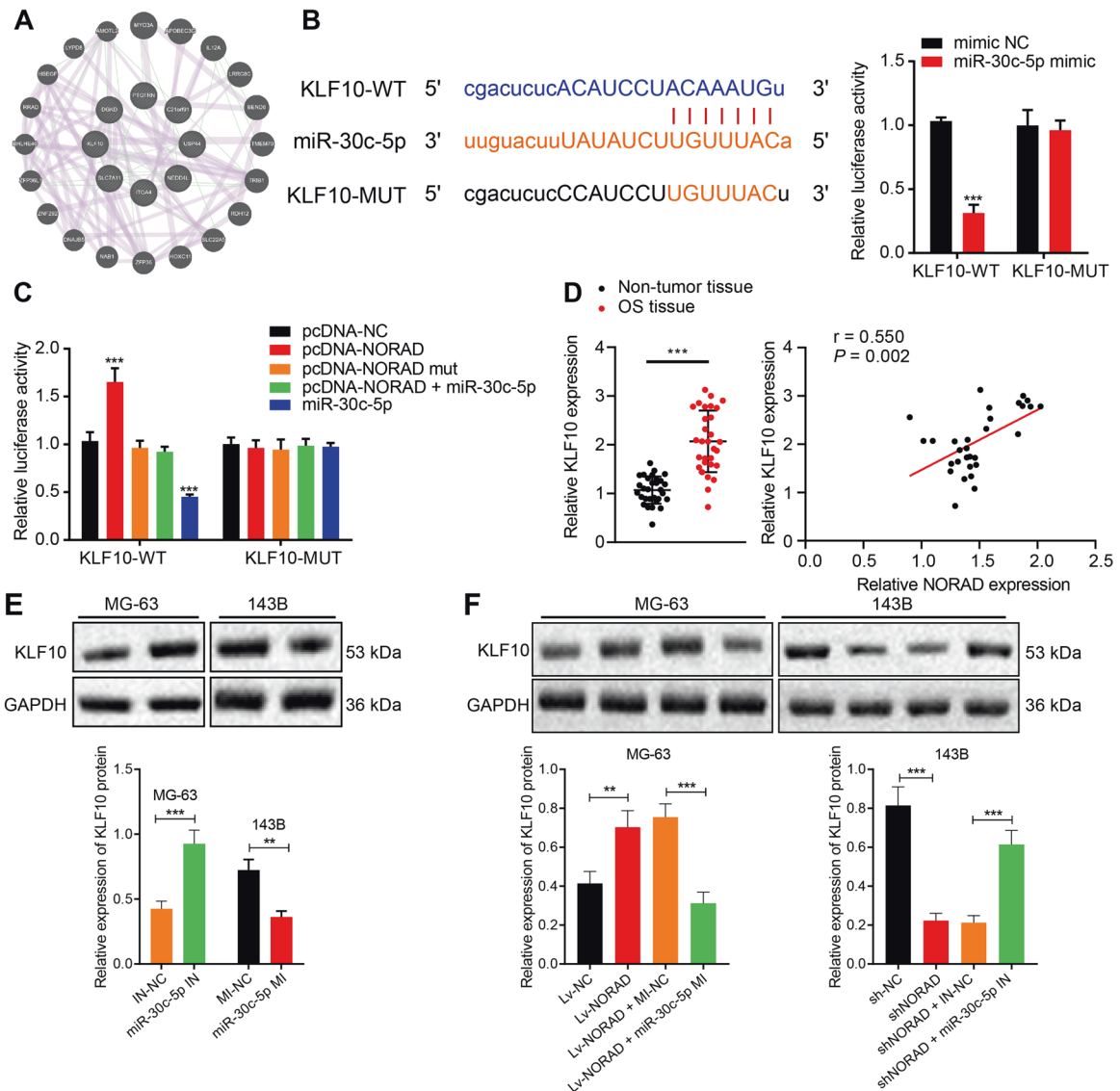


**Fig. 5** NORAD promoted KLF10 expression via sponging miR-30c-5p. **A** Analysis of gene-gene interaction. The inner circle represented 8 candidate genes, and the outer circle represented the genes interacting with these 8 genes. **B** The binding site of KLF10 and miR-30c-5p was predicted through starbase, and luciferase reporters were constructed to detect the luciferase activity in HEK-293T cells. **C** WT-NORAD, MUT-NORAD, miR-30c-5p, and WT/MUT-KLF10 luciferase reporter were used to analyze the luciferase activity in 143B cells. **D** The relative expression of KLF10 in osteosarcoma tissues and adjacent tissues was detected by RT-qPCR (left), and the correlation between NORAD level and KLF10 expression in osteosarcoma tissues was analyzed by Spearman (right) ( $n = 30$ ). **E** Western blot analysis showing KLF10 protein expression in osteosarcoma cells transfected with miR-30c-5p mimic/inhibitor. **F** Western blot analysis showing KLF10 protein expression in osteosarcoma cells after NORAD overexpression/knockdown or combined with miR-30c-5p mimic/inhibitor. The measurement data were expressed as mean  $\pm$  standard deviation. The comparison between cancer tissues and adjacent tissues was examined by paired *t* test. The comparison between other two groups was examined by unpaired *t* test, and the comparison of multiple groups of data was examined by one-way ANOVA, followed by Tukey's post hoc test. \* $p < 0.05$ , \*\* $p < 0.01$ , \*\*\* $p < 0.001$  vs. mimic NC, pcDNA-NC, or adjacent tissues. The experiment was repeated at least 3 times independently.

about significant inhibition of their proliferation and invasion abilities *in vitro* and *in vivo* [22]. Meanwhile, NORAD is also known to target the miR-410-3p to confer effects on drug resistance in osteosarcoma [39]. In regard to osteosarcoma, the danger of the malignancy is ascertained to metastasis, which is a complex multi-step process. Adhesion molecules, angiogenic factors, proteolytic enzymes, tumor metastasis-associated factors, and metastasis inhibitors are known to be involved in the process of migration and metastasis [40]. More importantly, NORAD can regulate metastasis; for instance, inhibition of NORAD by the YAP pathway suppresses lung and breast cancer metastasis by chelating S100P [41]. In our study, we revealed

that NORAD delivered by BMSC-derived EVs promoted the lung metastasis of osteosarcoma in nude mouse models.

Last but not the least, miRNAs are known to regulate gene expression through post-transcriptional regulation of mRNAs [42]. More remarkably, lncRNAs and miRNAs can communicate and co-regulate with each other in the ceRNA network [43]. For instance, NORAD was previously highlighted to drive the proliferation and migration of malignant cells in osteosarcoma *via* sponging miR-199a-3p [22]. We witnessed a similar relationship in our study, wherein NORAD functioned as a ceRNA of miR-30c-5p, while inhibition of miR-30c-5p facilitated metastasis and cancer cell proliferation in osteosarcoma. Largely in agreement with our

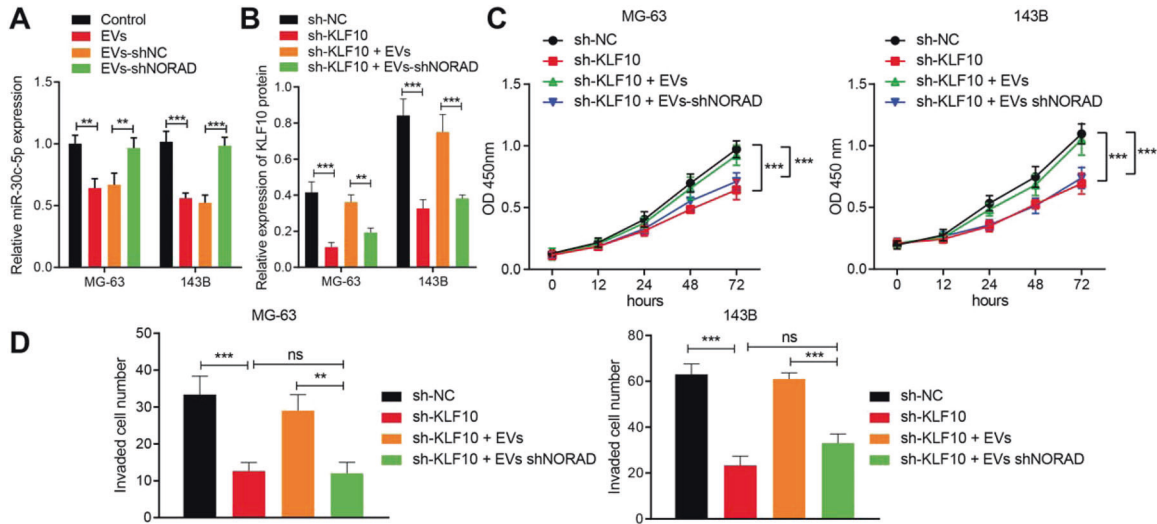


**Fig. 6** EV-NORAD promoted the proliferation and invasion of osteosarcoma cells via miR-30c-5p/KLF10 axis. **A** RT-qPCR showing miR-30c-5p expression in osteosarcoma cells treated with EVs or EV-shNORAD. **B** Western blot analysis showing KLF10 expression in osteosarcoma cells transfected with shKLF10 or further incubated with EVs or EV-shNORAD. **C** CCK-8 showing the proliferation of osteosarcoma cells transfected with shKLF10 or further incubated with EVs or EV-shNORAD. **D** Transwell showing the invasion of osteosarcoma cells transfected with shKLF10 or further incubated with EVs or EV-shNORAD. Scale bar, 50  $\mu$ m. The measurement data were expressed as mean  $\pm$  standard deviation. The comparison of multiple groups of data was examined by one-way ANOVA. Two-way ANOVA was used for comparison between groups at multiple time points, followed by Tukey's post hoc test. \* $p < 0.05$ , \*\* $p < 0.01$ , \*\*\* $p < 0.001$  vs. shNC. The experiment was repeated at least 3 times independently.

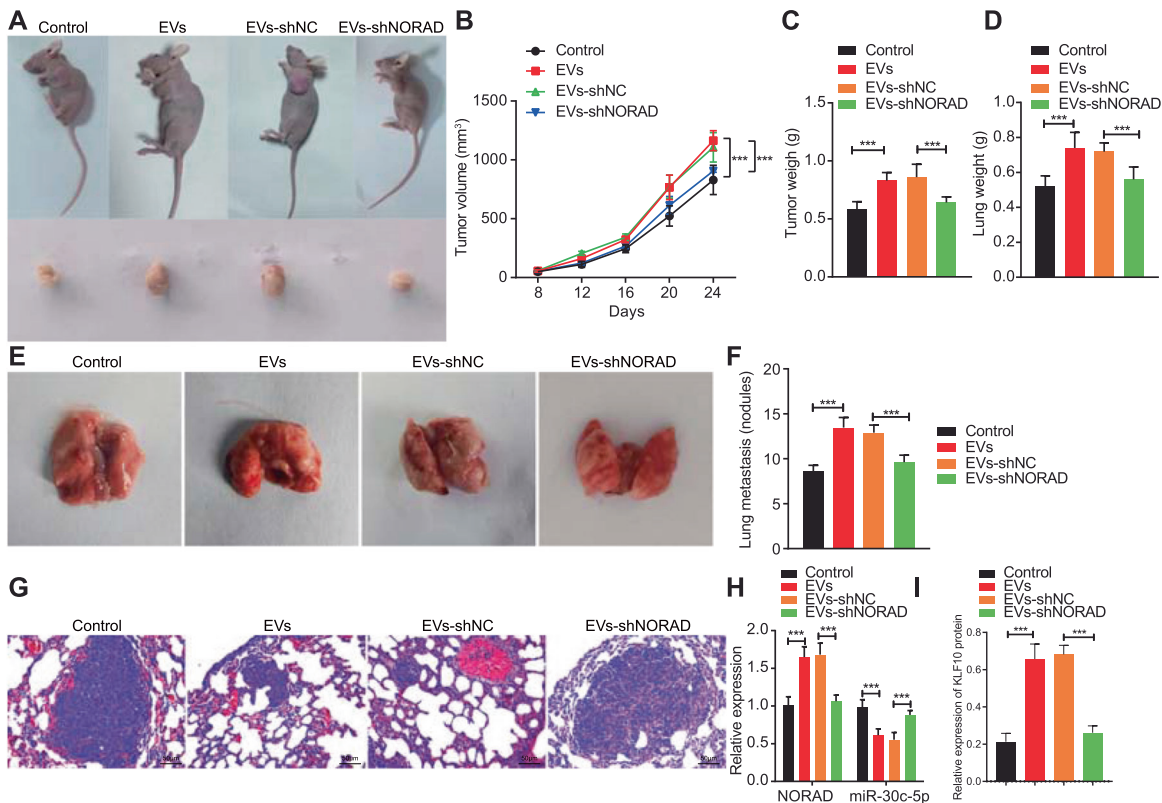


**Fig. 7** NORAD from BMSC-EVs promoted lung metastasis of osteosarcoma. **A** Representative macroscopic images of subcutaneous xenograft tumor from nude mice injected with EVs or EV-shNORAD,  $n = 10$ . **B** Volume of transplanted tumor from nude mice injected with EVs or EV-shNORAD at different time points,  $n = 10$ . **C** Weight of subcutaneous tumor from nude mice injected with EVs or EV-shNORAD,  $n = 10$ . **D** Weight of lung in nude mice injection with different osteosarcoma cells from nude mice injected with EVs or EV-shNORAD,  $n = 10$ . **E** Representative images of lung metastases from nude mice injected with EVs or EV-shNORAD. **F** The number of metastatic pulmonary nodules from nude mice injected with EVs or EV-shNORAD,  $n = 10$ . **G** HE staining showing metastatic lung nodules from nude mice injected with EVs or EV-shNORAD. Scale bar, 50  $\mu$ m. **H** RT-qPCR showing the expression of NORAD and miR-30c-5p in lung tissues from mice injected with EVs or EV-shNORAD,  $n = 10$ . **I** Western blot analysis showing KLF10 expression in lung tissues from mice injected with EVs or EV-shNORAD,  $n = 10$ . The measurement data were expressed as mean  $\pm$  standard deviation. The comparison of multiple groups of data was examined by one-way ANOVA. Repeated measures ANOVA was used for comparison between groups at multiple time points, followed by Tukey's post hoc test. \*\*\* $p < 0.001$ . The experiment is repeated at least 3 times independently.

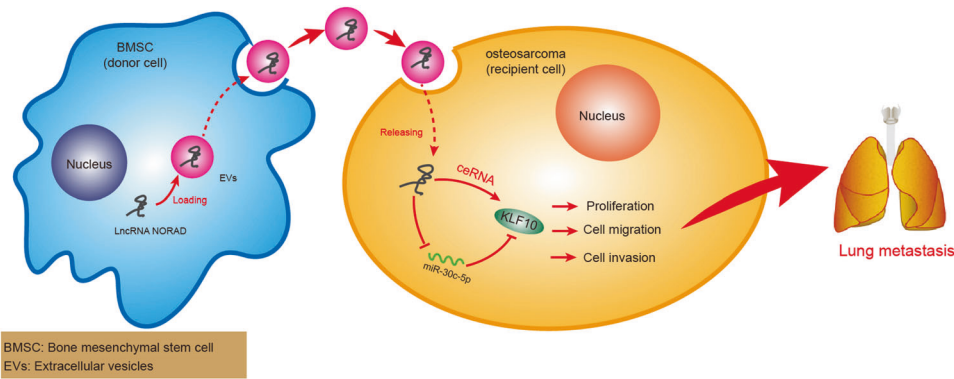


**Fig. 8** BMSC-EVs transferred NORAD to osteosarcoma cells. NORAD acted as a sponge of miR-30c-5p to promote KLF10 expression, thereby promoting osteosarcoma cell proliferation, migration, invasion, and lung metastasis.

results, several studies have documented the downregulation of miR-30c-5p in multiple malignancies such as breast, lung, and gastric tumors [44–46]. Moreover, a recent study found that miR-30c-5p was poorly expressed in osteosarcoma, and further lncRNA RP11-361F15.2 acted as a ceRNA against miR-30c-5p to regulate CPEB4, thereby promoting osteosarcoma tumorigenesis [21]. LncRNA PVT1 encapsulated in BMSC-derived EVs has been documented to facilitate growth and metastasis in osteosarcoma partly by sponging miR-183-5p [17]. Notably, lncRNA CASC15 loaded in osteosarcoma plasma EVs has been deciphered to enhance growth and metastasis of osteosarcoma cells by mediating the miR-338-3p/RAB14 axis [47]. Similar with these findings, we unearthed that co-culture with BMSC-EVs brought about declined miR-30c-5p levels, and that miR-30c-5p bound to KLF10, where inhibition of KLF10 decreased the malignant characteristics of osteosarcoma cells. KLF10, a target gene for multiple signaling pathways, is associated with cellular differentiation, and even highlighted as a potential marker for many human diseases, such as breast cancer, cardiac hypertrophy, and osteoporosis [48]. Further in line with our study, one recent report demonstrated that ceRNA mechanism underlying up-regulation of KLF10 promoted the growth and invasion of osteosarcoma cells [49]. Nevertheless, another study has suggested the functional role of tumor EV-educated MSCs in osteosarcoma progression, which identifies other targets, i.e., interleukin-6 and transforming growth factor- $\beta$  [50]. Hence, further investigation on other molecular mechanisms responsible for the function of BMSC-EVs is necessary.

Altogether, findings obtained in the current study indicated that NORAD promoted the progression of osteosarcoma, while EVs derived from BMSCs transported NORAD into osteosarcoma cells, thereby regulating the miR-30c-5p/KLF10 axis. This study provides evidence for a mechanism by which BMSC-EVs and NORAD promote the development of osteosarcoma, shedding light on prospective NORAD-based therapy against osteosarcoma.

#### AVAILABILITY OF DATA AND MATERIALS

The data that support the findings of this study are available from the corresponding authors upon reasonable request.

#### REFERENCES

- Jawad, M. U., Cheung, M. C., Clarke, J., Koniari, L. G. & Scully, S. P. Osteosarcoma: improvement in survival limited to high-grade patients only. *J. Cancer. Res. Clin. Oncol.* **137**, 597–607 (2011).
- Maran, A., Yaszemski, M.J., Kohut, A. & Voronov, A. Curcumin and osteosarcoma: can invertible polymeric micelles help? *Materials (Basel)* **9**, (2016)
- Hameed, M. & Mandelker, D. Tumor syndromes predisposing to osteosarcoma. *Adv. Anat. Pathol.* **25**, 217–222 (2018).
- Ottaviani, G. & Jaffe, N. The epidemiology of osteosarcoma. *Cancer Treat. Res.* **152**, 3–13 (2009).
- Pakos, E. E. et al. Prognostic factors and outcomes for osteosarcoma: an international collaboration. *Eur. J. Cancer* **45**, 2367–2375 (2009).
- Longhi, A. et al. Height as a risk factor for osteosarcoma. *J. Pediatr. Hematol. Oncol.* **27**, 314–318 (2005).
- Lindsey, B. A., Markel, J. E. & Kleinerman, E. S. Osteosarcoma overview. *Rheumatol. Ther.* **4**, 25–43 (2017).
- Reed, D. R. et al. Treatment pathway of bone sarcoma in children, adolescents, and young adults. *Cancer* **123**, 2206–2218 (2017).
- Harrison, D. J., Geller, D. S., Gill, J. D., Lewis, V. O. & Gorlick, R. Current and future therapeutic approaches for osteosarcoma. *Expert Rev. Anticancer Ther.* **18**, 39–50 (2018).
- Xie, L., Ji, T. & Guo, W. Anti-angiogenesis target therapy for advanced osteosarcoma (Review). *Oncol. Rep.* **38**, 625–636 (2017).
- Cortini, M., Avnet, S. & Baldini, N. Mesenchymal stroma: role in osteosarcoma progression. *Cancer Lett.* **405**, 90–99 (2017).
- Verrecchia, F. & Redini, F. Transforming growth factor- $\beta$  signaling plays a pivotal role in the interplay between osteosarcoma cells and their micro-environment. *Front. Oncol.* **8**, 133 (2018).
- Zheng, Y., Wang, G., Chen, R., Hua, Y. & Cai, Z. Mesenchymal stem cells in the osteosarcoma microenvironment: their biological properties, influence on tumor growth, and therapeutic implications. *Stem Cell Res. Ther.* **9**, 22 (2018).
- Tkach, M. & Thery, C. Communication by extracellular vesicles: where we are and where we need to go. *Cell* **164**, 1226–1232 (2016).
- Zhang, X. et al. Hypoxic BMSC-derived exosomal miRNAs promote metastasis of lung cancer cells via STAT3-induced EMT. *Mol. Cancer* **18**, 40 (2019).
- Qi, J. et al. Exosomes derived from human bone marrow mesenchymal stem cells promote tumor growth through hedgehog signaling pathway. *Cell Physiol. Biochem.* **42**, 2242–2254 (2017).
- Zhao, W. et al. Long non-coding RNA PVT1 encapsulated in bone marrow mesenchymal stem cell-derived exosomes promotes osteosarcoma growth and metastasis by stabilizing ERG and sponging miR-183-5p. *Aging (Albany NY)* **11**, 9581–9596 (2019).
- Yang, Z. et al. Noncoding RNA activated by DNA damage (NORAD): Biologic function and mechanisms in human cancers. *Clin. Chim. Acta* **489**, 5–9 (2019).
- Prensner, J. R. & Chinnaiyan, A. M. The emergence of lncRNAs in cancer biology. *Cancer Discov.* **1**, 391–407 (2011).
- Li, P. et al. MicroRNA-30c-5p inhibits NLRP3 inflammasome-mediated endothelial cell pyroptosis through FOXO3 down-regulation in atherosclerosis. *Biochem Biophys Res Commun* **503**, 2833–2840 (2018).
- Yang, D. et al. LncRNA RP11-361F15.2 promotes osteosarcoma tumorigenesis by inhibiting M2-like polarization of tumor-associated macrophages of CPEB4. *Cancer Lett.* **473**, 33–49 (2020).
- Wang, X. et al. Long noncoding RNA NORAD regulates cancer cell proliferation and migration in human osteosarcoma by endogenously competing with miR-199a-3p. *IUBMB Life* **71**, 1482–1491 (2019).
- Bing, Z. et al. Effect of mechanical stretch on the expressions of elastin, LOX and Fibulin-5 in rat BMSCs with ligament fibroblasts co-culture. *Mol. Biol. Rep.* **39**, 6077–6085 (2012).
- Puzar Dominkus, P. et al. PKH26 labeling of extracellular vesicles: Characterization and cellular internalization of contaminating PKH26 nanoparticles. *Biochim. Biophys. Acta Biomembr.* **1860**, 1350–1361 (2018).

25. Guo, Y., Rubin, E. M., Xie, J., Zi, X. & Hoang, B. H. Dominant negative LRP5 decreases tumorigenicity and metastasis of osteosarcoma in an animal model. *Clin. Orthop. Relat. Res.* **466**, 2039–2045 (2008).
26. Yuan, J. et al. Osteoblastic and osteolytic human osteosarcomas can be studied with a new xenograft mouse model producing spontaneous metastases. *Cancer Invest.* **27**, 435–442 (2009).
27. Pietrovito, L. et al. Bone marrow-derived mesenchymal stem cells promote invasiveness and transendothelial migration of osteosarcoma cells via a mesenchymal to amoeboid transition. *Mol. Oncol.* **12**, 659–676 (2018).
28. Lazennec, G. & Jorgensen, C. Concise review: adult multipotent stromal cells and cancer: risk or benefit? *Stem Cells* **26**, 1387–1394 (2008).
29. Fontanella, R. et al. A novel antagonist of CXCR4 prevents bone marrow-derived mesenchymal stem cell-mediated osteosarcoma and hepatocellular carcinoma cell migration and invasion. *Cancer Lett.* **370**, 100–107 (2016).
30. Kalluri, R. The biology and function of exosomes in cancer. *J. Clin. Invest.* **126**, 1208–1215 (2016).
31. Du, L. et al. CXCR1/Akt signaling activation induced by mesenchymal stem cell-derived IL-8 promotes osteosarcoma cell anoikis resistance and pulmonary metastasis. *Cell Death Dis.* **9**, 714 (2018).
32. Chen, A. K., Reuveny, S. & Oh, S. K. Application of human mesenchymal and pluripotent stem cell microcarrier cultures in cellular therapy: achievements and future direction. *Biotechnol. Adv.* **31**, 1032–1046 (2013).
33. Raab-Traub, N. & Dittmer, D. P. Viral effects on the content and function of extracellular vesicles. *Nat. Rev. Microbiol.* **15**, 559–572 (2017).
34. Qin, F. et al. Bone marrow-derived mesenchymal stem cell-derived exosomal microRNA-208a promotes osteosarcoma cell proliferation, migration, and invasion. *J. Cell Physiol.* **235**, 4734–4745 (2020).
35. Baglio, S. R. et al. Human bone marrow- and adipose-mesenchymal stem cells secrete exosomes enriched in distinctive miRNA and tRNA species. *Stem Cell Res. Ther.* **6**, 127 (2015).
36. Jones, K. B. et al. miRNA signatures associate with pathogenesis and progression of osteosarcoma. *Cancer Res.* **72**, 1865–1877 (2012).
37. Wang K, Jiang W, Cheng C, Li Y, Tu M. Pathological and therapeutic aspects of long noncoding RNAs in osteosarcoma. *Anticancer Agents Med. Chem.* (2017)
38. Smolle MA, Pichler M. The role of long non-coding RNAs in Osteosarcoma. *Noncoding RNA*, **4**, (2018)
39. Xie, X. et al. LncRNA NORAD targets miR-410-3p to regulate drug resistance sensitivity of osteosarcoma. *Cell Mol. Biol. (Noisy-le-grand)* **66**, 143–148 (2020).
40. Yang, Z. et al. Long noncoding RNAs in the progression, metastasis, and prognosis of osteosarcoma. *Cell Death Dis.* **7**, e2389 (2016).
41. Tan, B. S. et al. LncRNA NORAD is repressed by the YAP pathway and suppresses lung and breast cancer metastasis by sequestering S100P. *Oncogene* **38**, 5612–5626 (2019).
42. Iqbal, M. A., Arora, S., Prakasam, G., Calin, G. A. & Syed, M. A. MicroRNA in lung cancer: role, mechanisms, pathways and therapeutic relevance. *Mol. Aspects Med.* **70**, 3–20 (2019).
43. Tay, Y., Rinn, J. & Pandolfi, P. P. The multilayered complexity of ceRNA crosstalk and competition. *Nature* **505**, 344–352 (2014).
44. Pei, B. et al. Downregulation of microRNA-30c-5p was responsible for cell migration and tumor metastasis via COTL1-mediated microfilament arrangement in breast cancer. *Gland Surg.* **9**, 747–758 (2020).
45. Zhou, Y. et al. LncRNA DLEU2 modulates cell proliferation and invasion of non-small cell lung cancer by regulating miR-30c-5p/SOX9 axis. *Aging (Albany NY)* **11**, 7386–7401 (2019).
46. Cao, J. M., Li, G. Z., Han, M., Xu, H. L. & Huang, K. M. MiR-30c-5p suppresses migration, invasion and epithelial to mesenchymal transition of gastric cancer via targeting MTA1. *Biomed Pharmacother* **93**, 554–560 (2017).
47. Zhang, H. et al. LncRNA CASC15 is upregulated in osteosarcoma plasma exosomes and CASC15 knockdown inhibits osteosarcoma progression by regulating miR-338-3p/RAB14 Axis. *Onco. Targets Ther.* **13**, 12055–12066 (2020).
48. Subramaniam, M., Hawse, J. R., Rajamannan, N. M., Ingle, J. N. & Spelsberg, T. C. Functional role of KLF10 in multiple disease processes. *Biofactors* **36**, 8–18 (2010).
49. Wang, L. et al. Circ-0003998 promotes cell proliferative ability and invasiveness by binding to miR-197-3p in osteosarcoma. *Eur. Rev. Med. Pharmacol. Sci.* **23**, 10638–10646 (2019).
50. Baglio, S. R. et al. Blocking tumor-educated MSC paracrine activity halts osteosarcoma progression. *Clin. Cancer Res.* **23**, 3721–3733 (2017).

### AUTHOR CONTRIBUTIONS

Conceived and designed research: HH, WZ, PY; Performed experiments: HH, MD, TL; Analyzed data: WZ; Interpreted results of experiments: HH, MD, TL; Prepared figures: LZ; Drafted paper: HH, MD, TL, WZ; Edited and revised paper: LZ, WZ, PY; Approved final version of paper: HH, MD, TL, WZ, LZ, WZ, PY.

### COMPETING INTERESTS

The authors declare no competing interests.

### ADDITIONAL INFORMATION

**Supplementary information** The online version contains supplementary material available at <https://doi.org/10.1038/s41374-021-00691-6>.

**Correspondence** and requests for materials should be addressed to Wei Zhang.

**Reprints and permission information** is available at <http://www.nature.com/reprints>

**Publisher's note** Springer Nature remains neutral with regard to jurisdictional claims in published maps and institutional affiliations.